Talanta 99 (2012) 799–810

Contents lists available at SciVerse ScienceDirect

Talanta

journal homepage: www.elsevier.com/locate/talanta

Characterizing the gas phase ion chemistry of an ion trap mobility spectrometry based explosive trace detector using a tandem mass spectrometer ☆

Joseph Kozole [a,b], Jill Tomlinson-Phillips [a], Jason R. Stairs [a,*], Jason D. Harper [a,b], Stefan R. Lukow [a], Richard T. Lareau [a], Hacene Boudries [c], Hanh Lai [c], Carolyn S. Brauer [a]

[a] US Department of Homeland Security, Science &Technology Directorate, Transportation Security Laboratory, Atlantic City International Airport, NJ 08405, USA
[b] Nova Research, Inc., 1900 Elkin Street, Suite 230, Alexandria, VA 22308, USA
[c] Morpho Detection, Inc., 205 Lowell Street, Wilmington, MA 01887, USA

ARTICLE INFO

Article history:
Received 3 April 2012
Received in revised form
6 July 2012
Accepted 9 July 2012
Available online 26 July 2012

Keywords:
Explosives trace detector (ETD)
Ion trap mobility spectrometry (ITMS)
Tandem mass spectrometry (MS)
Density functional theory (DFT)
Gas phase ion chemistry

ABSTRACT

A commercial-off-the-shelf (COTS) ion trap mobility spectrometry (ITMS) based explosive trace detector (ETD) has been interfaced to a triple quadrupole mass spectrometer (MS/MS) for the purpose of characterizing the gas phase ion chemistry intrinsic to the ITMS instrument. The overall objective of the research is to develop a fundamental understanding of the gas phase ionization processes in the ITMS based ETD to facilitate the advancement of its operational effectiveness as well as guide the development of next generation ETDs. Product ion masses, daughter ion masses, and reduced mobility values measured by the ITMS/MS/MS configuration for a suite of nitro, nitrate, and peroxide containing explosives are reported. Molecular formulas, molecular structures, and ionization pathways for the various product ions are inferred using the mass and mobility data in conjunction with density functional theory. The predominant product ions are identified as follows: $[TNT\text{-}H]^-$ for trinitrotoluene (TNT), $[RDX+Cl]^-$ for cyclo-1,3,5-trimethylene-2,4,6-trinitramine (RDX), $[NO_3]^-$ for ethylene glycol dinitrate (EGDN), $[NG+NO_3]^-$ for nitroglycerine (NG), $[PETN+NO_3]^-$ for pentaerythritol tetranitrate (PETN), $[HNO_3+NO_3]^-$ for ammonium nitrate (NH_4NO_3), $[HMTD-NC_3H_6O_3+H+Cl]^-$ for hexamethylene triperoxide diamine (HMTD), and $[(CH_3)_2CNH_2]^+$ for triacetone triperoxide (TATP). The predominant ionization pathways for the formation of the various product ions are determined to include proton abstraction, ion-molecule attachment, autoionization, first-order and multi-order thermolysis, and nucleophilic substitution. The ion trapping scheme in the reaction region of the ITMS instrument is shown to increase predominant ion intensities relative to the secondary ion intensities when compared to non-ion trap operation.

Published by Elsevier B.V.

1. Introduction

Ion mobility spectrometry (IMS) based explosive trace detectors (ETDs) are well established screening devices for the mitigation of explosive related threats [1–5]. The utility of IMS for the detection of explosive residues is derived from the sensitivity and selectivity inherent to the analytical method. Specifically, the sensitivity and selectivity in IMS is imparted by the efficient processes which gas phase neutrals are converted to charged species, i.e. atmospheric pressure ionization, combined with the characterization of ion velocity through a buffer gas in the presence of an electric field, i.e. ion mobility measurements.

The most critical aspect of the IMS method is arguably the atmospheric pressure ionization processes since ion mobility measurements have no practical value if ions representative of the sample are not formed [5]. The molecular structures, kinetics, and thermodynamics which govern the ionization processes are dependent on the chemical environment in the IMS instrument, including temperature, pressure, gas composition, analyte concentration, moisture, and reagent chemical [5–11]. Therefore, a fundamental understanding of the effect these parameters have on the ionization pathways, ionization probabilities, and

☆ All opinions expressed in this paper are the author's and do not necessarily reflect the policies and view of the Department of Homeland Security, Transportation Security Laboratory, Department of Energy, or Oak Ridge Institute for Science and Education. References herein to any specific commercial products, processes, equipment, or services does not constitute or imply its endorsement, recommendation, or favoring by the United States Government or the Department of Homeland Security, or any of its employees or contractors.

* Corresponding author. Tel.: +1 609 813 2895.
E-mail address: jason.stairs@dhs.gov (J.R. Stairs).

0039-9140/$ - see front matter Published by Elsevier B.V.
http://dx.doi.org/10.1016/j.talanta.2012.07.030

ion stabilities in an IMS based ETD can be leveraged to improve the sensitivity and selectivity of existing IMS based equipment as well as guide the development of next generation mass spectrometry (MS) based equipment which utilizes atmospheric pressure ionization.

In an effort to gain fundamental insight into the gas phase ion chemistry intrinsic to IMS based ETDs, a platform that directly measures the mass-to-charge ratios, collision-induced dissociation pathways, and reduced mobility values for the ion species formed in an IMS based ETD has been developed and reported in a recent publication [12]. This platform involved the integration of a commercial-off-the shelf (COTS) IMS based ETD to the front-end of a triple quadrupole mass spectrometer. While the efficacy of this IMS/MS/MS configuration for the accurate characterization of the ion chemistry of that particular IMS system was demonstrated, the operating principles of the IMS system are not necessarily representative of all COTS IMS based ETDs. For example, the COTS IMS based ETD in the previously described IMS/MS/MS configuration utilizes an electrostatic ion shutter to gate the ions from the region where ionization occurs (reaction region) to the region where the ion mobility measurement is performed (drift region). Conversely, the COTS ion trap ion mobility (ITMS) based ETD described herein utilizes the electric field in the reaction region to accumulate and subsequently transfer the ions into the drift region; hence, the nomenclature variation "ion trap mobility spectrometry" [13–15].

The ion shutter in a conventional IMS instrument is located between the reaction and drift regions and is composed of a set of grids situated orthogonal to the path of the ions [1,5,16,17]. During the operation of the instrument, the electric field in the reaction region is set to continually direct the ions of a desired polarity toward the drift region. When a potential difference is applied between the grids in the ion shutter (i.e. the ion shutter is closed) the ions collide with the grids and become neutralized. However, when the potential applied to the grids is the same (i.e. the ion shutter is open) the ions pass into the drift region. Because the ion shutter is closed for ~99% of the experiment cycle, the majority of the ions formed in a conventional IMS instrument is discarded [5,13,18].

In contrast to the ion shutter configuration, an ITMS instrument maintains an electric field free space between the electrode at the inlet of the reaction region and the electrode between the reaction and drift regions to allow the ions to accumulate in the reaction region. Periodically, a voltage gradient is applied across the reaction region to introduce the ion population into the drift region. In principle, the gating scheme in the ITMS instrument eliminates the loss of ions due to the experimental cycle of an ion shutter, leading to a substantial increase in the density and residence time of the ions in the reaction region of the ITMS instrument compared to a conventional IMS instrument [13,14]. This increase in ion density and residence time, in addition to variations in temperature, composition, moisture, and reagent chemical between the COTS IMS based ETD in the previously described IMS/MS/MS instrument and the COTS ITMS based ETD, introduces the potential for different gas phase ionization processes in the ITMS instrument [13]. For this reason, direct characterization of the ion species formed in the ITMS instrument is necessary to develop a fundamental understanding of the gas phase ion chemistry intrinsic to the device.

In this manuscript, a method for interfacing a COTS ITMS based ETD to a triple quadrupole mass spectrometer is described and the ion masses, daughter ion masses, and reduced mobility values for the product ions formed from a suite of nitro, nitrate, and peroxide containing explosives are reported. Molecular formulas for the product ions from the various explosives are inferred using the sample composition along with the mass and mobility data obtained with the ITMS/MS/MS instrument while molecular structures for the predominant product ions are proposed using density functional theory calculations guided by the molecular formulas. Ionization pathways for the formation of the various product ions are discussed in detail, with part of the discussion focused on the influence ion trapping in the reaction region has on the ionization processes.

2. Materials and methods

2.1. Instrumentation

A schematic of the ITMS/MS/MS instrument is depicted in Fig. 1. The instrument is comprised of a COTS ITMS based ETD, an interface region, and a triple quadrupole mass spectrometer.

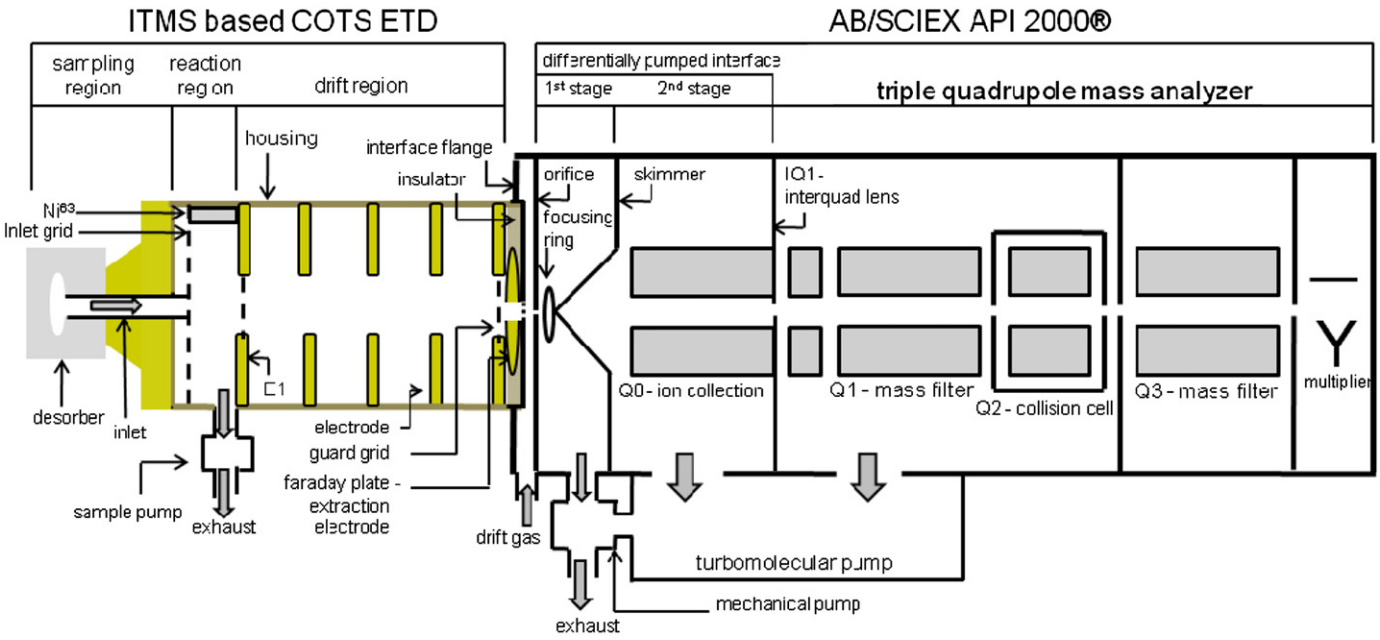

Fig. 1. Schematic of the ITMS/MS/MS instrument.

2.1.1. Ion trap mobility spectrometry based explosive detector

The COTS ITMS based ETD used in the ITMS/MS/MS instrument was manufactured by Morpho Detection Inc [13–15]. The operating parameters for the ITMS instrument are reported in Table 1. The ITMS instrument is composed of a thermal desorber, which is used to vaporize the sample, and an aluminum oxide housing containing a reaction region with a ^{63}Ni radiation source, an ambient pressure drift region, and a faraday plate detector, which are used to ionize, separate, and detect the sample vapor, respectively.

To analyze a sample using the ITMS instrument, a polytetrafluoroethylene (PTFE) filter (Morpho Detection Inc. Part M0001166-E) dosed with particle analyte is inserted into the desorber, the analyte is vaporized, and the vapor is directed into the reaction region using a diaphragm pump attached to the outlet on the ITMS housing between the reaction and drift regions. In the reaction region, positive and negative reactant ions, which are generated by the interaction of ^{63}Ni radiation with ammonia and dichloromethane doped purified air, react with the analyte vapor to form positive and negative product ions, respectively. Normally, an electric field free space is maintained between the inlet grid and the first ring electrode (E1 electrode), allowing reactant and products ions of both positive and negative polarity to accumulate in the reaction region. At 30 ms intervals, a voltage gradient is applied between the inlet grid and the E1 electrode for a duration of 0.2 ms, transferring the ions of a single polarity into the drift region. The polarity of the potential field is selected to introduce only the ions with the desired charge into the drift region, while the ions with the opposite charge travel toward the inlet grid and are neutralized. The drift region consists of several ring electrodes and a passive aperture grid integrated into the ITMS housing. The ions that enter the drift region are directed toward the aperture grid under the influence of a uniform electric field and separate based on their velocity through a counterflow drift gas of purified air. Subsequent to passing the aperture grid, the ions are detected using either the faraday plate or the mass spectrometer and the ion intensity is recorded relative to drift time to generate a mobility spectrum. The purified air used for the drift gas was house air treated with a purge gas generator (Parker Balston Model 75) and doped with ammonia (Real Sensors Part MP035087) and dichloromethane (VICI Metronics Part 100-100-4201-630) reagent chemicals. The purified air was measured to have a water content of 1–10 ppm using a moisture analyzer (General Electric Moisture Monitor Series 3) and a carbon dioxide content of 50–100 ppm using a carbon dioxide transmitter (Vaisala Series GMT 220). Note, only the hardware, and not the detection algorithms, for the ITMS instrument was used in the ion chemistry studies presented in this manuscript.

2.1.2. Interface region

The mass spectrometer used in the ITMS/MS/MS instrument is an API 2000 manufactured by AB/SCIEX [19]. A detailed depiction of the interface between the ITMS instrument and the mass spectrometer is displayed in Fig. 2 with dimensions and voltages reported in Table 1. The method used to interface the ITMS instrument to the mass spectrometer has been described elsewhere [12,20]. Briefly, an ITMS instrument without a faraday plate or the portion of the ITMS housing located after the guard grid was fabricated. The guard grid end of the modified ITMS instrument was connected to a custom interface flange using a fastening plate, bolts, and a PTFE o-ring. The custom interface flange was constructed from stainless steel and was designed to contain a custom faraday plate as well as attach to the atmospheric pressure interface of the mass spectrometer. The custom faraday plate was constructed by drilling a 5.5 mm hole into the center of the original faraday plate of the ITMS instrument. Before connecting the ITMS instrument to the interface flange, the faraday plate was positioned on the ITMS instrument side of the interface flange and was electrically isolated using an aluminum oxide insulator. A passive grid was welded to the mass spectrometer side of the interface flange to define the electric field between the faraday plate and the interface flange. The curtain plate was removed from the mass spectrometer and the interface flange was attached in its place such that the hole in the faraday plate was aligned with the pinhole in the orifice and that the interface flange and its grid were electrically isolated from the mass spectrometer. Electric contact was made with the faraday plate via a feedthrough on the interface flange.

During the operation of the ITMS/MS/MS instrument, the faraday plate is connected to either a current-to-voltage preamplifier (Morpho Detection Inc.) to measure a mobility spectrum or

Table 1
Operating parameters and dimensions for the ITMS/MS/MS instrument.

Parameter	Value	Unit	Parameter	Value	Unit
Electric Field Strength (ITMS)			**Dimensions (interface region)**		
Drift region	225	V/cm	Distance from guard grid to faraday plate	1.6	mm
Pressures			Distance from faraday plate to interface flange grid	4.4	mm
Reaction region/drift region	760	Torr	Distance from interface flange grid to orifice	3.8	mm
1st pumping stage	1	Torr	Distance from orifice to skimmer	3.3[a] or 6.3[b]	mm
2nd pumping stage	8[a] or 1[b]	10^{-3} Torr	Faraday plate hole size	5.5	mm
Mass spectrometer	8[a] or 4[b]	10^{-7} Torr	Orifice hole size	254	μm
Temperatures			Skimmer hole size	1100[a] or 400[b]	μm
Desorber	220	°C	[c]**Voltages (interface region)**		
Reaction region/drift region (housing)	162	°C	Guard grid	−257	V
Reaction region/drift region (i.e. exit gas temperature)	156	°C	Faraday plate	−200[a,b] or 0[d]	V
Orifice	165	°C	Interface flange/interface flange grid	−75	V
Gas flows			Orifice	−5[a] or −20[b]	V
Sample flow	50	cc/min	Skimmer	0[a] or −15[b]	V
[*]Drift gas	100	cc/min	Q0	5	V
			IQ1	6[a] or 15[b]	V

[a] Value for the acquisition of mass and MS/MS spectra.
[b] Value for the acquisition of mass-selected ion mobility spectra.
[c] Voltages are for negative mode operation. Voltages for positive mode operation are the same magnitude but opposite polarity.
[d] Value for the acquisition of mobility spectra at the faraday plate.
* Purified air (5–25 ppm water and 50–100 ppm carbon dioxide) doped with dichloromethane and ammonia reagent chemicals was used as the drift gas.

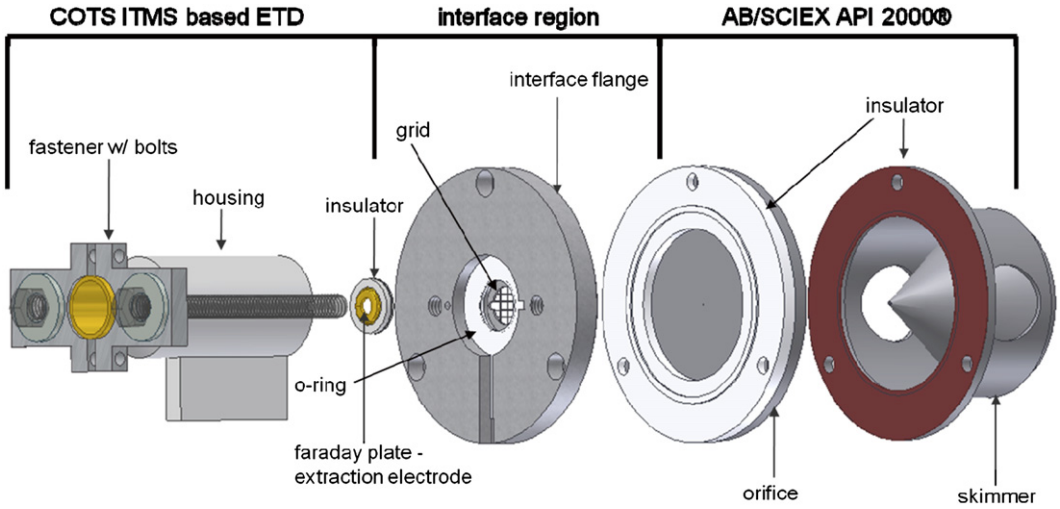

Fig. 2. Computer aided drawing of the interface region of the ITMS/MS/MS instrument.

a voltage power supply (EMCO High Voltage Model Q02) to extract the ion beam from the ITMS instrument toward the grid on the interface flange. In the case where the faraday plate is used to extract the ion beam, a potential is applied to the interface flange and its grid to pass the ions through the grid and into the mass spectrometer. The purified air for the drift gas is introduced into the interface region between the faraday plate and the orifice with a total flow of 700 cc/min (Omega Engineering Model FMA 1700), 600 cc/min of which is pulled into the vacuum of the mass spectrometer and 100 cc/min of which serves as the drift gas for the ITMS instrument [12,20].

2.1.3. Triple quadrupole mass spectrometer

The operating parameters for the API 2000 are reported in Table 1. The API 2000 is composed of a differentially pumped interface, which is used to transfer the ion beam from the atmospheric pressure to the vacuum of the mass spectrometer, and a triple quadrupole mass analyzer, which is used to filter and detect the ion beam [19]. The ion beam enters the initial pumping stage through the pinhole in the orifice electrode and is then guided through the skimmer electrode into an intermediate pumping stage via gas flow and an electric field between the orifice and skimmer. Upon entering the intermediate pumping stage, large scale collisions with the background gas in the radio frequency (rf) only quadrupole (Q0) focus the trajectory of the ion beam onto the centered axis of the quadrupoles in the mass analyzer (i.e. collisional focusing) [19,21]. The ion beam is transferred from the intermediate pumping stage to the triple quadrupole mass analyzer via an electric field between the skimmer and the mass analyzer. The components of the mass analyzer are a mass filter (Q1), a collision cell (Q2), a second mass filter (Q3), and an electron multiplier detector. The mass analyzer is operated in the scan only mode to acquire a mass spectrum, the product ion scan mode to acquire a tandem mass (MS/MS) spectrum, and the selected ion monitoring (SIM) scan mode to acquire a mobility spectrum for a particular m/z.

The skimmer in the differentially pumped interface was modified such that the electric field strength and pressure in the intermediate pumping stage (Q0 region) could be adjusted to values not permitted in the standard configuration of the mass spectrometer. In the standard configuration, the potential between the skimmer and Q0 (V_{s-Q0}) can only be varied from 0 to ± 12 V while the pressure in the Q0 region (P_{Q0}) is constant at 8 mTorr. To overcome the restrictions, the skimmer was electrically isolated from the chamber of the mass spectrometer using polyimide and connected to a voltage power supply (EMCO High Voltage Model Q01), allowing V_{s-Q0} to be varied from 0 V to ± 112 V. Additionally, the size of the opening in a skimmer electrode was reduced from 1100 μm to 400 μm, allowing P_{Q0} to be alternated between 8 and 1 mTorr by inserting into the mass spectrometer either a skimmer with the original 1100 μm hole size or the skimmer with the reduced 400 μm hole size, respectively.

The intermediate pumping stage is set to a V_{s-Q0} of 5 V and a P_{Q0} of 8 mTorr when the mass analyzer is used to acquire a mass or MS/MS spectrum and to a V_{s-Q0} of 20 V and a P_{Q0} of 1 mTorr when the mass analyzer is used to acquire a mobility spectrum. Decreased electric field strength and increased pressure in the Q0 region is optimal when acquiring a mass or MS/MS spectrum because the settings are ideal for collisional focusing, providing a higher transmission probability of the ion beam from the ITMS instrument to the mass analyzer and therefore a higher sensitivity measurement. At the same time, collisional focusing broadens and distorts the temporal profile of a discrete ion packet, preventing a mobility measurement using the mass analyzer. Conversely, increased electric field strength and decreased pressure in the Q0 region reduces the effect of collisional focusing and eliminates broadening and distortion of the ion packet, making the settings optimal for acquiring a mobility spectrum. A detailed description of collisional focusing in relation to the operating capabilities of an IMS/MS/MS instrument is provided elsewhere [12,20,22].

2.2. Data acquisition

2.2.1. Mobility spectra

To acquire a mobility spectrum at the faraday plate, ions are accumulated in the reaction region and periodically pulsed into the drift region using the electric field between the inlet grid and the E1 electrode (i.e. ion trapping and pulsing is implemented). The faraday plate is connected to a preamplifier and the ion intensity is recorded relative to drift time between the reaction region and the faraday plate using a high speed digitizer (National Instruments Model PXI 5124) with custom LabVIEW software (National Instruments).

2.2.2. Mass and MS/MS spectra with ion trapping

To acquire a mass or MS/MS spectrum in the ion trapping mode, ion trapping and pulsing is implemented in the reaction region, the faraday plate is connected to a voltage power supply

to extract the ion beam into the mass spectrometer, the intermediate pumping stage is tuned to decrease electric field strength and increase pressure settings, and the mass analyzer is operated in the scan only or product ion scan modes. The mass and MS/MS spectra are recorded using the Analyst software (AB/SCIEX).

2.2.3. Mass-selected ion mobility spectra

To acquire a mobility spectrum using the mass spectrometer, ion trapping and pulsing is implemented, the faraday plate is connected to a voltage power supply, the intermediate pumping stage is tuned to increase electric field strength and decrease pressure settings, and the mass analyzer is operated in the SIM mode to detect only the ions with a particular m/z. The intensity for the ion of interest is recorded relative to the drift time between the reaction region and the electron multiplier using a high speed digitizer (National Instruments Model PXI 5124) with custom LabVIEW software to provide a mass-selected mobility spectrum. A multiple mass mobility spectrum can be produced by summing the individual mass-selected mobility spectra for all reactant and product ions detected for a particular sample.

2.2.4. Mass and MS/MS spectra with continuous ion flow

To acquire a mass or MS/MS spectrum in the continuous ion flow mode, the electric field between the inlet grid and the E1 electrode is set to continually pass the ions formed in the reaction region into the drift region (i.e. ion trapping and pulsing is not implemented), the faraday plate is connected to a voltage power supply, the intermediate pumping stage is tuned to decrease electric field strength and increase pressure settings, and the mass analyzer is operated in the scan only or product ion scan modes. The continuous ion flow mode is used to simulate the conditions in the reaction region of the ITMS instrument if an ion shutter was to be implemented in place of the ion trapping scheme, and therefore can be used to determine the effect ion trapping may have on product ion formation in the ITMS instrument [18].

2.3. Sample preparation

Explosive samples were prepared by depositing dissolved explosive solutions onto PTFE filters and drying the aliquot under a flow of purified air. The concentrations of the dissolved explosive solutions were selected such that 1 μL aliquots of the solutions provided the desired sample amounts. The explosive samples studied in this manuscript include trinitrotoluene (TNT), cyclo-1,3,5-trimethylene-2,4,6-trinitramine (RDX), ethylene glycol dinitrate (EGDN), nitroglycerine (NG), pentaerythritol tetranitrate (PETN), ammonium nitrate (NH_4NO_3), hexamethylene triperoxide diamine (HMTD), and triacetone triperoxide (TATP). The TNT, RDX, EGDN, NG, and PETN solutions were obtained from AccuStandard while the NH_4NO_3, HMTD, and TATP solutions were obtained from the Transportation Security Laboratory. The TNT and RDX solutions were prepared in 1:1 methanol:acetonitrile, the NG solution was prepared in 1:1 methanol:ethanol, the PETN solution was prepared in methanol, the NH_4NO_3 solution was prepared in water, the EGDN and HMTD solutions were prepared in acetonitrile, and the TATP solution was prepared in hexane.

2.4. Density functional theory calculations

A series of density functional theory calculations were performed using the Gaussian 09 suite of programs [23,24]. The gas phase molecule of interest and molecular fragment ion geometries were optimized with the B3LYP functional using 6-311++G(2df,2p) basis sets. Vibrational and single-point energy calculations were performed at the same level of theory. The optimized structures contain no imaginary frequencies, indicating that each structure corresponds to a local minimum on the potential energy surface. Multiple starting structures were analyzed; most of the structures minimized to the most probable structure, while the few structures that demonstrated severe fragmentation were discarded, as they did not form stable ions. Natural bond orbital (NBO) analysis was performed on the HMTD fragment ions to explore the electron distribution into atomic and molecular orbitals to derive the molecular bonding of the fragment [25].

3. Results and discussion

3.1. Evaluation of the utility of the ITMS/MS/MS instrument

To illustrate the efficacy of the ITMS/MS/MS instrument for the characterization of the gas phase ion chemistry of the ITMS based ETD, mobility spectra acquired for 100 ng samples of RDX using both a benchtop ITMS instrument (Morpho Detection Inc.) and the ITMS/MS/MS instrument operated in the negative ion detection mode under identical conditions are displayed in Fig. 3. Fig. 3a is the mobility spectrum obtained using an ITMS instrument identical to the ITMS component of the ITMS/MS/MS instrument, Fig. 3b is the mobility spectrum obtained using the faraday plate in the ITMS/MS/MS instrument, Fig. 3c is the multiple mass mobility spectrum obtained using the electron multiplier in the ITMS/MS/MS instrument, and Fig. 3d is the mass-selected mobility spectra for $[Cl]^-$ at m/z 35, $[NO_2]^-$ at m/z 46, $[RDX+Cl]^-$ at m/z 257, and $[RDX+NO_2]^-$ at m/z 268 obtained using the ITMS/MS/MS instrument. The mobility spectra, along with all other spectra reported in the manuscript, are the averaged signal for a 10 s period following the start of sample desorption. The mobility spectra are plotted as a function of the inverse reduced mobility value to adjust for any variations

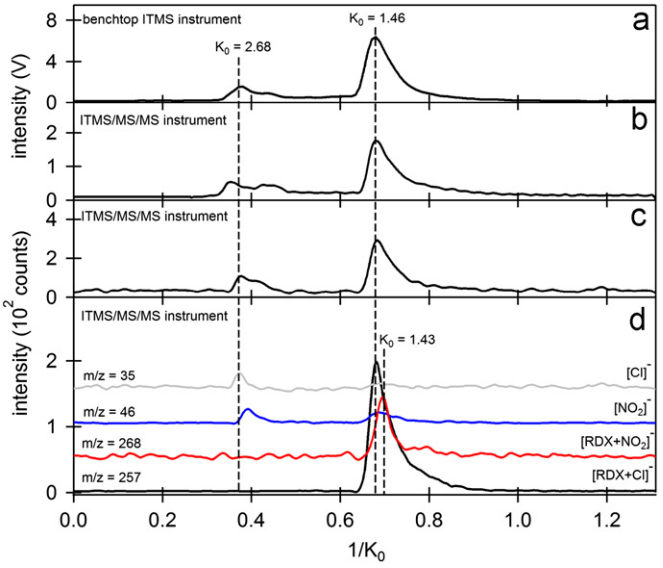

Fig. 3. Mobility spectra for 100 ng RDX samples acquired using a benchtop ITMS instrument and the ITMS/MS/MS instrument. Plot (a) is the mobility spectrum obtained using a benchtop ITMS instrument, plot (b) is the mobility spectrum obtained using the faraday plate in the ITMS/MS/MS instrument, plot (c) is a multiple mass mobility spectrum obtained using the ITMS/MS/MS instrument, and the plots in (d) are the individual mass-selected ion mobility spectra for $[Cl]^-$ at m/z 35 (gray), $[NO_2]^-$ at m/z 46 (blue), $[RDX+NO_2]^-$ at m/z 268 (red), and $[RDX+Cl]^-$ at m/z 257 (black) obtained using the IMS/MS/MS instrument. (For interpretation of the references to color in this figure legend, the reader is referred to the web version of this article.)

between the benchtop ITMS instrument and the ITMS/MS/MS instrument as well as the drift time between the faraday plate in the ITMS instrument and the electron multiplier in the mass spectrometer. The reduced mobility (K_0) value for an ion of interest was calculated using the equation:

$$K_0 = (t_d^{TNT} K_0^{TNT})/t_d \quad (1)$$

where t_d^{TNT} is the drift time for the explosive standard TNT (i.e. the reference compound), K_0^{TNT} is the reduced mobility value for TNT, and t_d is the drift time for the ion of interest [26]. The value for K_0^{TNT} was calculated to be 1.54 $cm^2\ V^{-1}\ s^{-1}$ using the equation:

$$K_0^{TNT} = (L/(Et_d^{TNT}))(273/T)(P/760) \quad (2)$$

where L is the length, E is the electric field strength, T is the temperature, and P is the pressure in the drift region of the ITMS instrument [26].

The mobility spectra acquired using the benchtop ITMS instrument (Fig. 3a), the faraday plate in the ITMS/MS/MS instrument (Fig. 3b), and the mass analyzer in the ITMS/MS/MS instrument (Fig. 3c) are nearly identical with respect to the number of peaks, the ratio in intensity between the peaks, the peak widths and shapes, and the K_0 values for the peaks. The similarity between the mobility spectra obtained using the benchtop ITMS instrument (Fig. 3a) and the faraday plate in the ITMS/MS/MS instrument (Fig. 3b) indicates that the ion chemistry of the ITMS instrument is unaltered subsequent to being interfaced to the mass spectrometer, whereas, the similarity between the spectra obtained using the faraday plate (Fig. 3b) and the mass analyzer (Fig. 3c) in the ITMS/MS/MS instrument in addition to the measurement of the intact $[RDX+Cl]^-$ and $[RDX+NO_2]^-$adduct ions with the mass analyzer indicates that the core structures of the ions formed in the ITMS instrument do not undergo large-scale reactions or fragmentation (except for clustering and declustering of water molecules) during transfer from the ITMS instrument to the mass spectrometer [5,27]. The mass-selected ion mobility spectra (Fig. 3d) determine that the K_0 values for $[RDX+Cl]^-$ and $[RDX+NO_2]^-$ are 1.46 and 1.43 $cm^2\ V^{-1}\ s^{-1}$ respectively, which is in agreement with the K_0 values previously reported for the product ions of RDX [2,7,28–30], indicating that the ITMS/MS/MS instrument is useful for the simultaneous measurement of mass and mobility. Collectively, the above observations validate the efficacy of the ITMS/MS/MS instrument for the accurate characterization of the ion chemistry of the ITMS based ETD.

3.2. Characterization of the gas phase ion chemistry of the ITMS instrument

To characterize the gas phase ion chemistry of the ITMS based ETD, a series of mass, MS/MS, mobility, and mass-selected mobility spectra for the explosives TNT, RDX, EGDN, NG, PETN, NH_4NO_3, HMTD, and TATP were acquired using the ITMS/MS/MS instrument. Mass and MS/MS spectra for RDX, NG, PETN, NH_4NO_3, HMTD, and TATP are displayed in Figs. 4 and 5 while mobility and mass-selected mobility spectra for PETN, NH_4NO_3, HMTD, and TATP are displayed in Fig. 6. Sample amounts were 100 ng for RDX and 250 ng for NG, PETN, NH_4NO_3, HMTD, and TATP. The spectrum for TATP was obtained in the positive ion detection mode while the spectra for all other explosives were obtained in the negative ion detection mode. The ITMS component of the ITMS/MS/MS instrument was operated in the ion trapping mode for the acquisition of all spectra. The MS/MS spectra were acquired by flooding the collision cell with nitrogen to a pressure of 1 Torr and scanning the collision energy between 5 and 40 eV. The ions targeted for the MS/MS and mass-selected mobility

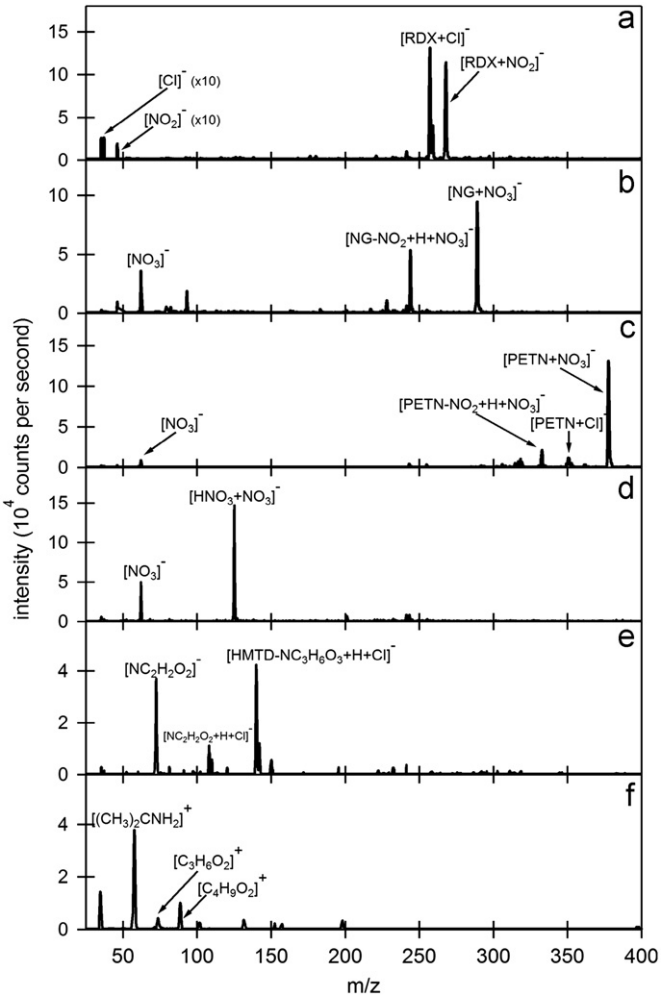

Fig. 4. Mass spectra from the analysis of a 100 ng RDX sample (a), a 250 ng NG sample (b), a 250 ng PETN sample (c), a 250 ng NH_4NO_3 sample (d), a 250 ng HMTD sample (e), and a 250 ng TATP sample (f) obtained using the ITMS/MS/MS instrument in the ion trapping mode.

spectra were chosen using the mass spectra (Fig. 4) to identify the m/z for all ions formed during the analysis of each explosive.

A summary of the molecular formulas, ion masses, daughter ion masses, and K_0 values for the product ions from the analysis of the various explosives is provided in Table 2. The molecular formulas for the product ions were inferred using the sample composition along with the ion masses from the mass spectra, the daughter ion masses from the MS/MS spectra, and the K_0 values from the mobility and mass-selected mobility spectra. The K_0 values for RDX, EGDN, NG, PETN, NH_4NO_3, and HMTD were calculated using Eq. (1). The K_0 values for TATP were calculated using Eq. (1) with cocaine serving in place of TNT as the reference. The K_0 value for cocaine was calculated to be 1.16 $cm^2\ V^{-1}\ s^{-1}$ using Eq. (2). Comments regarding the relative intensities and ionization processes for the product ions are included in the notes column of Table 2.

Calculated molecular structures for the NG, PETN, HMTD, and TATP molecules as well as the $[NG+Cl]^-$, $[NG+NO_3]^-$, $[PETN+Cl]^-$, $[PETN+NO_3]^-$, $[HNO_3+NO_3]^-$, $[HMTD-NC_3H_6O_3+H+Cl]^-$, and $[(CH_3)_2CNH_2]^+$ product ions are displayed in Fig. 7. The molecular structures were calculated using density functional theory guided by the molecular formulas inferred from the sample composition, ion masses, daughter ion masses, and K_0 values (Table 2).

Together, the mobility and mass measurements made using the ITMS/MS/MS instrument and the calculations performed

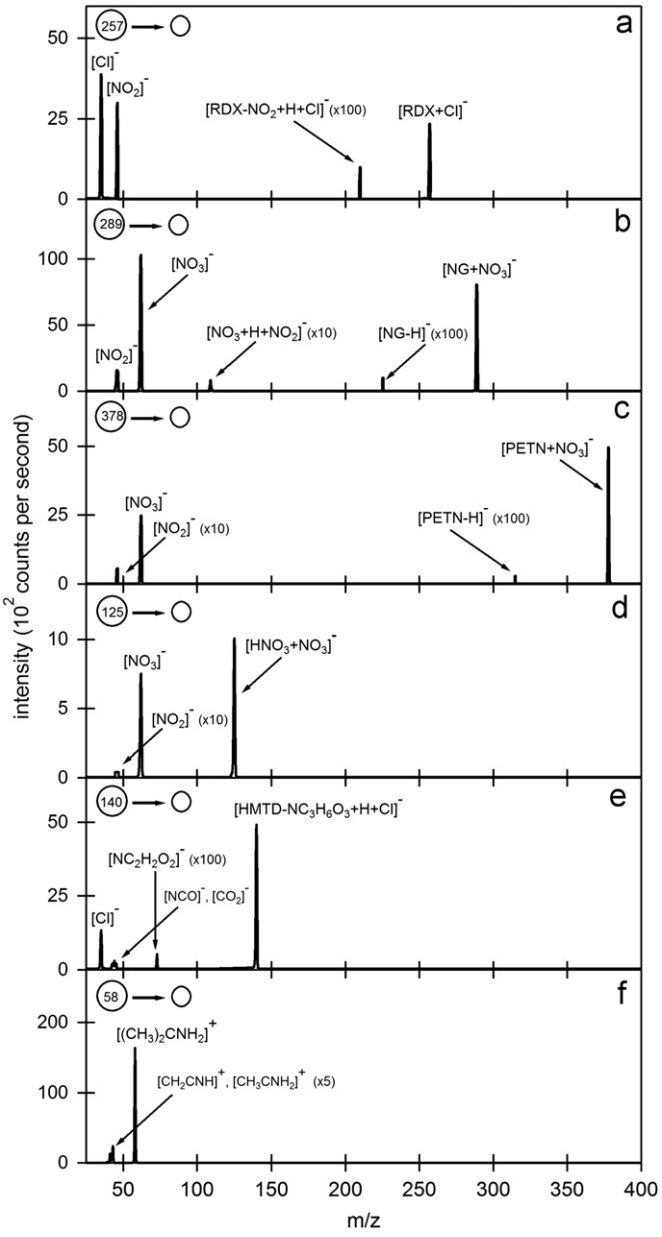

Fig. 5. MS/MS spectra for $[RDX+Cl]^-$ at m/z 257 (a), $[NG+NO_3]^-$ at m/z 289 (b), $[PETN+NO_3]^-$ at m/z 378 (c), $[HNO_3+NO_3]^-$ at m/z 125 (d), $[HMTD-NC_3H_6O_3+H+Cl]^-$ at m/z 140 (e), and $[(CH_3)_2CNH_2]^+$ at m/z 58 (f) obtained using the ITMS/MS/MS instrument in the ion trapping mode.

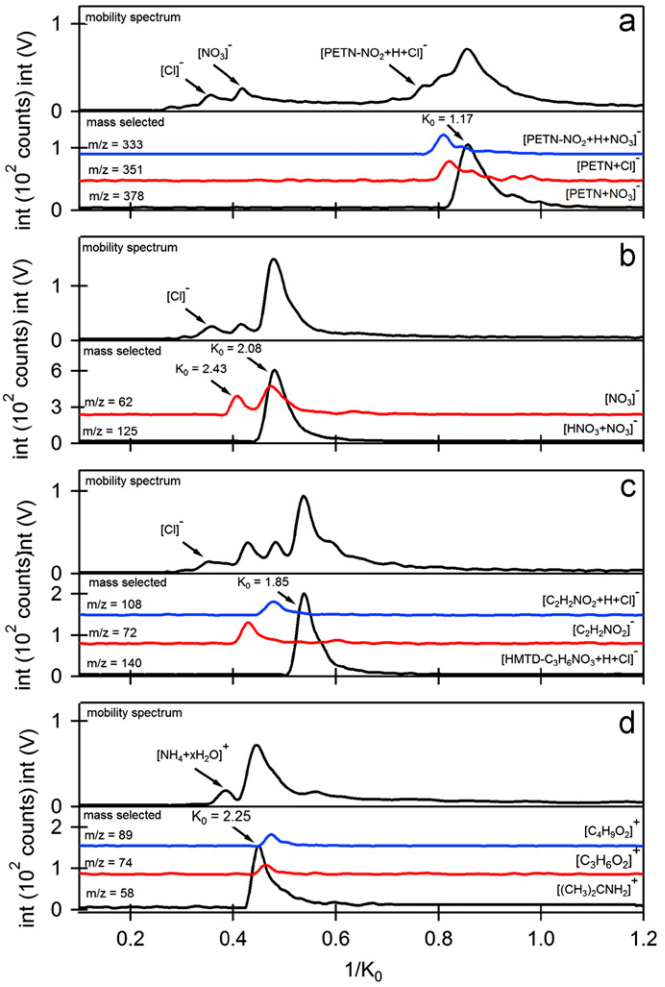

Fig. 6. Mobility (top plots) and mass-selected (bottom plots) mobility spectra from the analysis of a 250 ng PETN sample (a), a 250 ng NH_4NO_3 sample (b), a 250 ng HMTD sample (c), and a 250 ng TATP sample (d) obtained using the ITMS/MS/MS instrument.

using density functional theory lead to several conclusions regarding the gas phase ionization processes in an ITMS based ETD. Overall, the predominant product ions for TNT, RDX, EGDN, NG, PETN, NH_4NO_3, HMTD, and TATP in the ITMS based ETD are determined to be $[TNT-H]^-$, $[RDX+Cl]^-$, $[NO_3]^-$, $[NG+NO_3]^-$, $[PETN+NO_3]^-$, $[HNO_3+NO_3]^-$, $[HMTD-NC_3H_6O_3+H+Cl]^-$, and $[(CH_3)_2CNH_2]^+$, respectively. Secondary product ions include $[NO_2]^-$ and $[RDX+NO_2]^-$ for RDX, $[NO_3]^-$, $[NG-NO_2+H+Cl]^-$, $[NG-NO_2+H+NO_3]^-$, and $[NG+Cl]^-$ for NG, $[NO_3]^-$, $[PETN-NO_2+H+Cl]$, $[PETN-NO_2+H+NO_3]^-$, and $[PETN+Cl]^-$ for PETN, $[NO_3]^-$ for NH_4NO_3, $[NC_2H_2O_2]^-$ and $[NC_2H_2O_2+H+Cl]^-$ for HMTD, and $[C_3H_6O_2]^+$ and $[C_4H_9O_2]^+$ for TATP. The following discussion, which is aided by experimental and computational findings from the literature, describes the ionization processes responsible for the formation of the various product ions. Note that the product ion species and ionization pathways are specific to the operating parameters of the ITMS instrument and may change if different reagent chemicals, temperatures, moisture levels, or carbon dioxide levels are implemented during the operation of the device.

Product ion formation at atmospheric pressure is largely dependent on the chemical composition and temperature in the reaction medium [5–11]. The reaction region in the ITMS instrument is primarily composed of nitrogen (N_2) and oxygen (O_2) gas with part per million (ppm) level water (H_2O), ammonia (NH_3), and dichloromethane (CH_2Cl_2), in addition to high and low energy electrons (e^-), N_2^+, $H^+ \cdot xH_2O$, and $O_2^- \cdot xH_2O$ intermediate ions, and $NH_4^+ \cdot xH_2O$ and $Cl^- \cdot xH_2O$ reactant ions. Ionization pathways for the formation of the $H^+ \cdot xH_2O$, and $O_2^- \cdot xH_2O$ intermediate ions and the $NH_4^+ \cdot xH_2O$ and $Cl^- \cdot xH_2O$ reactant ions from the supporting reaction environment have been reported elsewhere [5,28]. Because the enthalpy ($\Delta_f H$) for proton attachment favors formation of NH_4^+ ($\Delta_f H = -853$ kJ/mol) over H_3O^+ ($\Delta_f H = -703$ kJ/mol) and the enthalpy for electron attachment favors the formation of Cl^- ($\Delta_f H = -347$ kJ/mol) over O_2^- ($\Delta_f H = -42$ kJ/mol) [9,10,29,30], $NH_4^+ \cdot xH_2O$ and $Cl^- \cdot xH_2O$ serve as the main source for charge transfer during product ion formation in the positive and negative ion channels, respectively. For simplicity, the $NH_4^+ \cdot xH_2O$ and $Cl^- \cdot xH_2O$ reactant ions will be denoted as $[NH_4]^+$ and $[Cl]^-$ for the remainder of the discussion. The temperatures (Table 1) for the sample desorber, reaction region, and drift region in the

Table 2
Summary of the molecular formulas, ion masses, daughter ion masses, and calculated and literature reduced mobility values for the product ions formed during the analysis of TNT, RDX, EGDN, NG, PETN, NH_4NO_3, HMTD, and TATP.

Sample	Product ion formula	Ion mass (amu)	Daughter ion mass—Formula	K_0 measured ($cm^2\ V^{-1}\ s^{-1}$)	K_0 literature ($cm^2\ V^{-1}\ s^{-1}$)	Notes
TNT	[a]$[TNT-H]^-$	226	→46—$[NO_2^-]$ 136–$[TNT-3NO]^-$ 166—$[TNT-2NO]^-$ 183—$[TNT-NO_2]^-$ 196—$[TNT-NO]^-$	1.54	1.59[b] [50] 1.54 [2,9,37] 1.48 [45]	-Major intensity -Proton abstraction reaction
RDX	$[NO_2]^-$	46	–	2.68	–	-Minor to moderate intensity -Decomposition
RDX	[a]$[RDX+Cl]^-$	257, 259	→35—$[Cl]^-$ 46—$[NO_2]^-$ 210—$[RDX-NO_2+H+Cl]^-$ $NO_2+H+Cl]^-$	1.46	1.48[b] [50] 1.40 [2,45]	-Major intensity-Ion–molecule attachment reaction
RDX	$[RDX+NO_2]^-$	268	→46—$[NO_2]^-$ 221—$[RDX-H]^-$	1.43	1.43 [2] 1.42[b] [50]	-Moderate to major intensity -Autoionization reaction
EGDN NG PETN NH_4NO_3	$[NO_3]^-$	62	–	2.43	2.46 [2] 2.48 [51]	-Minor to major intensity -Predominant ion for EGDN -Decomposition
NG	$[NG\text{-}NO_2+H+Cl]^-$	217, 219	→35—$[Cl]^-$ 46—$[NO_2]^-$ 62—$[NO_3]^-$ 109—$[NO_3+NO_2+H]^-$	1.64	–	-Trace intensity -Ion-molecule attachment reaction
NG	$[NG-NO_2+H+NO_3]^-$	244	→46—$[NO_2]^-$ 62—$[NO_3]^-$ 226—$[NG-H]^-$	1.45	–	-Minor to moderate intensity -Ion–molecule attachment reaction
NG	$[NG+Cl]^-$	262, 264	→35—$[Cl]^-$ 46—$[NO_2]^-$ 62—$[NO_3]^-$ 109—$[NO_3+NO_2+H]^-$ 226—$[NG\text{-}H]^-$	1.44	–	-Minor intensity -Ion–molecule attachment reaction
NG	[a]$[NG+NO_3]^-$	289	→46—$[NO_2]^-$ 62—$[NO_3]^-$ 109—$[NO_3+NO_2+H]^-$ 226—$[NG\text{-}H]^-$	1.33	1.32 [2], 1.37 [37]	-Major intensity-Autoionization reaction
PETN	$[PETN-NO_2+H+Cl]^-$	306, 308	→ 35—$[Cl]^-$ 46—$[NO_2]^-$ 62—$[NO_3]^-$ 109—$[NO_3+NO_2+H]^-$	1.29	–	-Minor intensity -Ion–molecule attachment reaction
PETN	$[PETN-NO_2+H+NO_3]^-$	333	→62–$[NO_3]^-$ 109—$[NO_3+NO_2+H]^-$ 315—$[PETN\text{-}H]^-$	1.24	–	-Minor intensity -Ion–molecule attachment reaction
PETN	$[PETN+Cl]^-$	351, 353	→35—$[Cl]^-$ 46—$[NO_2]^-$ 62—$[NO_3]^-$ 109—$[NO_3+NO_2+H]^-$ 315—$[PETN-H]^-$	1.22	1.15 [1,2,52]	-Minor intensity -Ion–molecule attachment
PETN	[a]$[PETN+NO_3]^-$	378	→46—$[NO_2]^-$ 62–$[NO_3]^-$ 315–$[PETN-H]^-$	1.17	1.19 [50], 1.10 [1,2], 1.09 [52]	-Major intensity -Autoionization reaction
NH_4NO_3	[a]$[HNO_3+NO_3]^-$	125	→46—$[NO_2]^-$ 62–$[NO_3]^-$	2.08	-	-Major intensity -Autoionization reaction
HMTD	$[NC_2H_2O_2]^-$	72	→26—$[CN]^-$ 42—$[NCO]^-$ 44—$[CO_2]^-$	2.32	2.42 [11]	-Minor to moderate intensity -Decomposition
HMTD	$[NC_2H_2O_2+H+Cl]^-$	108, 110	→35—Cl]$^-$ 42—$[NCO]^-$ 44—$[CO_2]^-$ 72—$[NC_2H_2O_2]^-$	2.08	–	-Minor intensity -Decomposition followed by ion–molecule attachment reaction
HMTD	[a][HMTD-$NC_3H_6O_3+H+Cl]^-$	140, 142	→35—$[Cl]^-$ 42—$[NCO]^-$ 44—$[CO_2]^-$ 72—$[NC_2H_2O_2]^-$	1.85	1.88 [11]	-Major intensity -Decomposition followed by ion–molecule attachment reaction
TATP	[a]$[(CH_3)_2CNH_2]^+$	58	→41—$[CH_2CNH]^+$ 43—$[CH_3CNH_2]^+$	2.25	2.32 [11]	-Major intensity -Nucleophilic substitution reaction
TATP	$[C_3H_6O_2]^+$	74	→43—$[C_2H_3O]^+$	2.16	–	-Minor intensity -Decomposition
TATP	$[C_4H_9O_2]^+$	89	→43—$[C_2H_3O]^+$ 47—$[C_2H_7O]^+$	2.12	2.18 [11]	-Minor intensity

[a] Predominant ion.
[b] Ion not mass identified.

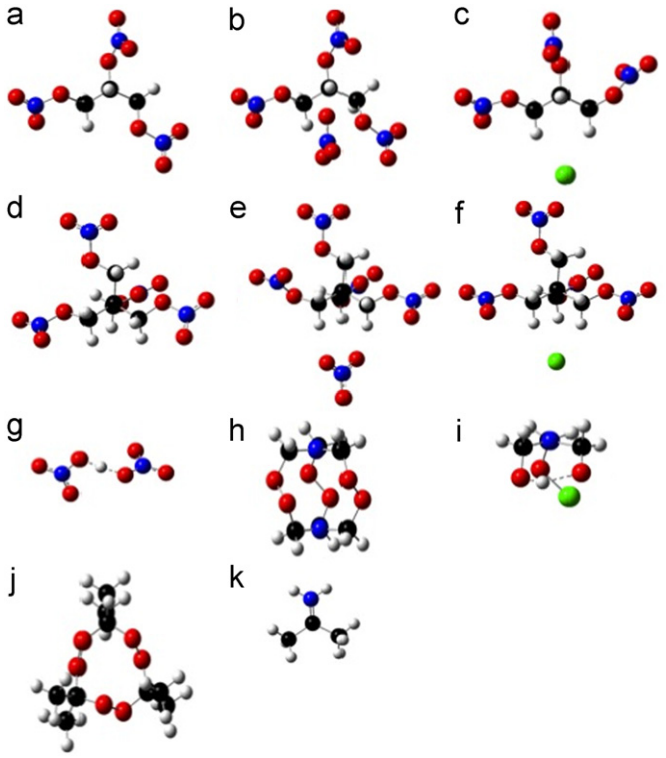

Fig. 7. Optimized density functional theory structures obtained at the B3LYP/G6-311 level for NG (a), $[NG+NO_3]^-$ (b), $[NG+Cl]^-$ (c), PETN (d), $[PETN+NO_3]^-$ (e), $[PETN+Cl]^-$ (f), $[HNO_3+NO_3]^-$ (g), HMTD (h), $[HMTD-NC_3H_6O_3+H+Cl]^-$ (i), TATP (j), and $[(CH_3)_2CNH_2]^+$ (k).

ITMS instrument are maintained above the decomposition temperatures for all explosives studied except TNT, introducing the potential for thermolysis of the analyte molecules during sample introduction, product ion formation, and ion mobility separation [2,31–34].

In a reaction environment consistent with the ITMS instrument, it is well established that the $[TNT-H]^-$ product ion is formed via abstraction of a proton from a TNT molecule by $[Cl]^-$ (i.e. a proton abstraction reaction) [9,35], the $[RDX+Cl]^-$, $[NG+Cl]^-$, and $[PETN+Cl]^-$ product ions are formed via $[Cl]^-$ attachment to RDX, NG, and PETN molecules (i.e. an ion–molecule attachment reaction) [2,7,36], and the $[RDX+NO_2]^-$, $[NG+NO_3]^-$, and $[PETN+NO_3]^-$ are formed via $[NO_x]^-$ attachment to RDX, NG, and PETN molecules (i.e. an autoionization reaction) [31,36,37]. For the autoionization of RDX, the NO_2 fragment is generated by first-order thermolysis of a N–NO_2 bond in the molecule, a favorable pathway considering the bond dissociation energy (D_E) for the N–NO_2 bond ($D_{E\ N-NO_2} = 163$ kJ/mole) is smaller than any other bond in the molecule (D_E other ≥ 305 kJ/mole) and roughly equal to the activation energy (E_A) for vaporization ($E_{A\ RDX} = 131$ kJ/mole) [31,38,39]. Production of the NO_2 fragment by thermolysis of the RDX molecule is supported by the observation that the ion intensity for $[RDX+NO_2]^-$ relative to $[RDX+Cl]^-$ decreased by a factor of 3 when the temperature for the sample desorber was decreased from 220 °C to 160 °C. For the autoionization of NG and PETN, formation of the NO_3 fragment by the first-order thermolysis of a C–ONO_2 bond in the nitrate ester molecules seems unlikely given the bond dissociation energy is larger for the C–ONO_2 bond ($D_{E\ C-ONO_2} = 332$ kJ/mole) than the O–NO_2 bond ($D_{E\ O-NO_2} = 183$ kJ/mole) [40]. Instead, the pathway for the formation of NO_3 from nitrate esters may involve multi-order thermolysis, with dissociation of the O–NO_2 bond as the initiating step [40–43]. Production of the NO_3 fragment from PETN by thermolysis is supported by the bond dissociation energy for the O–NO_2 bond ($D_{E\ O-NO_2} = 183$ kJ/mole) being smaller than the activation energy for vaporization ($E_{A\ PETN} = 233$ kJ/mole) [31]. The statement is further substantiated by the observation that the ion intensity for $[PETN+NO_3]^-$ relative to $[PETN+Cl]^-$ decreased when the temperature for the thermal desorber was decreased. Conversion of the NO_2 and NO_3 fragments to $[NO_2]^-$ and $[NO_3]^-$ occurs by homolytic bond cleavage (i.e. radical formation) during the decomposition process and/or attachment of a low energy electron in the reaction region [39]. Production of $[NO_3]^-$ from EGDN likely follows the same pathway as the production of $[NO_3]^-$ from NG and PETN. The $[NG-NO_2+H+Cl]^-$, $[NG-NO_2+H+NO_3]^-$, $[PETN-NO_2+H+Cl]^-$, and $[PETN-NO_2+H+NO_3]^-$ secondary ions are proposed to be formed via $[Cl]^-$ or $[NO_3]^-$ attachment to incompletely nitrated NG or PETN molecules. The source of the incompletely nitrated nitrate ester molecules is impurities from a partial nitration process during sample synthesis and/or thermolysis during sample desorption.

The calculated molecular structures for the NG and PETN molecules (Fig. 7a and d) and the $[NG+Cl]^-$, $[NG+NO_3]^-$, $[PETN+Cl]^-$, and $[PETN+NO_3]^-$ product ions (Fig. 7b and c and e and f) indicate that the hydrogen atoms and nitrate functional groups bonded to the alpha carbon atoms in the nitrate ester molecules undergo reorientation in order to electrostatically interact with $[Cl]^-$ or $[NO_3]^-$ (i.e. form an adduct with $[Cl]^-$ or $[NO_3]^-$). The binding energies, distances, and angles between the nitrate ester molecules and $[Cl]^-$ or $[NO_3]^-$ satisfy the definition for hydrogen bonding (see Supplemental material) [46]. Reorientation of the hydrogen atoms and nitrate groups in the nitrate esters causes the C–ONO_2 bond to strengthen and the O–NO_2 bond to weaken, providing evidence that multi-order decomposition of the molecule may be initiated by dissociation of the O–NO_2 bond (see Supplemental material). The ion–molecule binding energies (B_E) for the $[NG+Cl]^-$ ($B_E = 117$ kJ/mole) and $[PETN+Cl]^-$ ($B_E = 138$ kJ/mole) adducts are calculated to be larger than the binding energies for the $[NG+NO_3]^-$ ($B_E = 96$ kJ/mole) and $[PETN+NO_3]^-$ ($B_E = 121$ kJ/mole) adducts, respectively. While $[Cl]^-$ adduct formation with nitrate esters is favored according to the calculations, the $[NG+NO_3]^-$ and $[PETN+NO_3]^-$ product ions are observed to be more abundant than the $[NG+Cl]^-$ and $[PETN+Cl]^-$ product ions when NG and PETN are analyzed using the ITMS instrument (Fig. 4 and Table 1). This discrepancy is attributed to $[NO_3]^-$ having a larger concentration than $[Cl]^-$ in the reaction region of the ITMS instrument during the analysis of nitrate esters. The statement is supported by the observation that the relative ion intensities for the $[NG+Cl]^-$ and $[PETN+Cl]^-$ product ions increased relative to the $[NG+NO_3]^-$ and $[PETN+NO_3]^-$ product ions when the concentration of dichloromethane in the reaction region was increased.

The ionization pathways for inorganic nitrates and organic peroxides at atmospheric pressure are less established compared to their organic nitro and nitrate counterparts. For NH_4NO_3, the $[HNO_3+NO_3]^-$ product ion is formed via thermolysis of the ionic compound to form nitric acid (HNO_3) followed by autoionization of the HNO_3 molecule with $[NO_3]^-$ [32,47]. The $[NO_3]^-$ fragment ion is generated from HNO_3 by thermolysis and/or reactions with the supporting environment. To confirm that the $[HNO_3+NO_3]^-$ product ion is formed via autoionization, the amount of NH_4NO_3 analyzed was varied from 1000 ng to 10 ng and the thermal desorber temperature was varied from 220 °C to 160 ° 1 The experiment showed that the ion intensity for $[HNO_3+NO_3]^-$ relative to $[NO_3]^-$ decreased as the sample amount and thermal desorber temperature was decreased, indicating that formation of $[HNO_3+NO_3]^-$ is more favorable when the amount of sample introduced into the reaction region is large and therefore the probability of a HNO_3 molecule interacting with a $[NO_3]^-$ is high.

For HMTD, it is proposed that the $[HMTD-NC_3H_6O_3+H+Cl]^-$ product ion is formed via homolytic thermolysis of all the three

peroxide bonds (i.e. O–O bonds) in the HMTD molecule followed by proton and $[Cl]^-$ attachment (see Supplemental material), whereas, the $[NC_2H_2O_2]^-$ and $[NC_2H_2O_2+H+Cl]^-$ secondary ions are formed via thermolysis of an N–C bond in the $NC_3H_6O_3$ decomposition product of HMTD [11,34,48]. Dissociation of the peroxide bonds followed by dissociation of a C–N bond is a favorable decomposition pathway for the HMTD molecule considering the O–O ($D_{E\ O-O}$=145 kJ/mole) and N–C ($D_{E\ N-C}$=308 kJ/mole) bonds have the smallest and next to the smallest bond dissociation energies in the molecule ($D_{E\ other} \geq 348$ kJ/mole) [48].

It has previously been shown by Ewing et al. that TATP vapor in the presence of ^{63}Ni radiation and excess ammonia yields a $[(CH_3)_2CNH_2]^+$ product ion via a nucleophilic substitution reaction between an NH_3 molecule and a $[TATP+NH_4]^+$ adduct [30]. In the substitution reaction, the NH_3 molecule serves as the nucleophile, the $[TATP+NH_4]^+$ adduct serves as the substrate, and the $C(CH_3)_2$ group in the TATP molecule serves as the electrophile (or leaving group). To confirm that this reaction pathway is taking place in the ITMS instrument, mass spectra for TATP ($C_9H_{18}O_6$), deuterium labeled TATP ($C_9D_{18}O_6$), and carbon 13 labeled TATP ($C_6^{13}C_3H_{18}O_6$, where only the ring carbons are labeled) were acquired using the ITMS/MS/MS instrument. The spectra showed that the product ion mass shifted from m/z 58 for TATP to m/z 64 for deuterium labeled TATP and m/z 59 for carbon 13 labeled TATP, indicating that the product ion contains 6 hydrogen atoms and 1 ring carbon from the TATP molecule, ultimately supporting the molecular formula assignment for the product ion as $[(CH_3)_2CNH_2]^+$ in addition to the nucleophilic substitution reaction pathway [49]. The molecular formula assignment and substitution reaction pathway for the $[(CH_3)_2CNH_2]^+$ product ion is further supported by the analysis of TATP with nitrogen 14 labeled ammonia reagent ($^{14}NH_3$), which yielded a product ion shift from m/z 58 to m/z 59, indicating that the product ion contains 1 nitrogen atom from the substitution of an amine group into the TATP molecule. The $[C_3H_6O_2]^+$ secondary ion for TATP is proposed to be formed via dissociation of the peroxide bonds in the TATP molecule while the pathway for the production of the $[C_4H_9O_2]^+$ secondary ion is undetermined; however, may involve formation of a peroxy radical. Similar to the $[(CH_3)_2CNH_2]^+$ product ion, the molecular formulas for the secondary ions were confirmed using isotopic labeling [49].

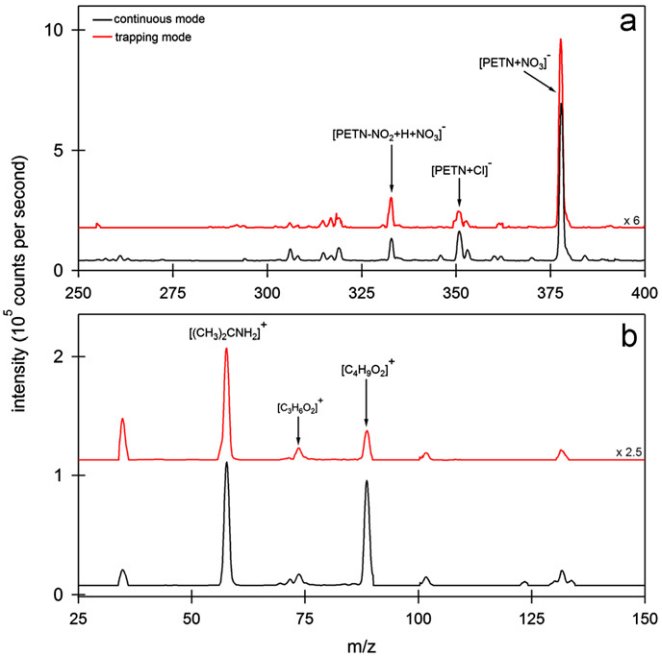

Fig. 8. Mass spectra from the analysis of a 250 ng PETN sample (a) and a 250 ng TATP sample (b) obtained using the ITMS/MS/MS instrument in the ion trapping (red plots) and continuous ion flow (black plots) modes. (For interpretation of the references to color in this figure legend, the reader is referred to the web version of this article.)

3.3. Evaluation of the effect of ion trapping on the gas phase ion chemistry of the ITMS instrument

To illustrate the effect ion trapping in the reaction region has on the gas phase ion chemistry in an ITMS based ETD, a comparison between mass spectra obtained using the ITMS/MS/MS instrument in the ion trapping and continuous ion flow modes is displayed in Fig. 8. The samples for the mass spectra were 250 ng PETN (Fig. 8a) and 250 ng TATP (Fig. 8b). Note that the intensities of the mass spectra obtained in the ion trapping mode have been multiplied by a factor of 6 for PETN and a factor of 2.5 for TATP. A summary of the absolute and relative intensities for the predominant and secondary product ions before normalization is provided in Table 3. Because the temperatures, pressures, gas flows, and electric field strengths were the same for the acquisition of the mass spectra in the different operating modes, any discrepancies in the absolute and relative intensities for the

Table 3
Summary of the absolute and relative intensities for the product ions formed during the analysis of PETN and TATP using the ITMS/MS/MS instrument in the ion trapping and continuous ion flow modes.

PETN				TATP			
Molecular formula	**Ion mass**	**Absolute intensity (counts)**	**Relative intensity (%)**	**Molecular formula**	**Ion mass**	**Absolute intensity (counts)**	**Relative intensity (%)**
Trapping mode				**Trapping mode**			
$[NO_3]^-$	62	1.1 E05	7.0	$[(CH_3)_2CNH_2]^+$	58	4.9 E05	100
$[PETN-NO_2+H+Cl]^-$	306, 308	5.8 E04	3.6	$[C_3H_6O_2]^+$	74	5.7 E04	11.7
$[PETN-NO_2+H+NO_3]^-$	333	1.8 E05	11.1	$[C_4H_9O_2]^+$	89	1.3 E05	27.0
$[PETN+Cl]^-$	351, 353	1.6 E05	9.9	**Continuous mode**			
$[PETN+NO_3]^-$	378	1.6 E06	100	$[(CH_3)_2CNH_2]^+$	58	1.4 E06	100
Continuous mode				$[C_3H_6O_2]^+$	74	1.3 E05	9.1
$[NO_3]^-$	62	5.8 E05	7.1	$[C_4H_9O_2]^+$	89	1.2 E06	86.2
$[PETN-NO_2+H+Cl]^-$	306, 308	6.1 E05	7.5	**Total ion intensity**			
				PETN—Continuous mode—1.2 E07, Trapping Mode—2.1 E06			
$[PETN-NO_2+H+NO_3]^-$	333	1.2 E06	14.2	**Ratio (continuous/trapping)—5.7**			
$[PETN+Cl]^-$	351, 353	1.5 E06	18.7	**TATP**—Continuous mode—2.7 E06, Trapping Mode—6.8 E05			
$[PETN+NO_3]^-$	378	8.1 E06	100	**Ratio (continuous/trapping)—4.0**			

reactant and product ions are credited to the ion trapping scheme in the ITMS instrument [18].

Two important differences are observed between the ion trapping and continuous ion flow operating modes. The first difference is the total ion intensities (i.e. the sum of the absolute intensities for all reactant and product ions) are larger in the continuous ion flow mode than the ion trapping mode by a factor of 5.7 for PETN and a factor of 4.0 for TATP. The larger absolute ion intensities in the continuous ion flow mode indicate that the ion trapping scheme in the ITMS instrument is $<100\%$ efficient, more specifically, only $\sim$18–25% of the ions generated are retained by the ion trap. The loss of ions in the ion trapping mode is attributed to neutralization via collisions with the components of the ITMS instrument, such as the inlet grid, E1 electrode, and ITMS housing, in addition to recombination in the reaction medium. Despite the $<100\%$ efficiency of the ion trapping scheme, the residence times in the reaction region for the ions that are retained by the ion trap are up to 1–2 orders of magnitude greater than the residence times for the ions generated during continuous ion flow operation. The larger residence times in the ion trapping mode are expected to lead to increased reaction times, ion densities, and ion–molecule interactions during product ion formation in the ITMS instrument.

The second difference between the ion trapping and continuous operating modes is the relative intensities for the secondary product ions are smaller in the ion trapping mode (i.e. the predominant ion intensities are larger relative to the secondary ion intensities in the ion trapping mode). For example, the relative intensities for the $[PETN+Cl]^-$ (from PETN) and $[C_4H_9O_2]^+$ (from TATP) secondary ions are 19% and 86% in the continuous ion flow mode and 10% and 27% in the ion trapping mode, respectively, or a factor of 2–3 smaller in the ion trapping mode. The increase in predominant ion intensity relative to secondary ion intensity in the ion trapping mode is attributed to increased reaction times, ion densities, and ion–molecule interactions in the reaction region driving the equilibrium of the reaction and charge transfer pathways further toward the products that are most favorable according to enthalpy of formation as well as temperature and composition of the supporting reaction environment.

4. Conclusions

A Morpho Detection ITMS based ETD has been successfully interfaced to a triple quadrupole mass spectrometer and the gas phase ion chemistry of the ITMS instrument for a list of nitro, nitrate, and peroxide containing explosives has been elucidated. The ITMS/MS/MS configuration has been demonstrated to be capable of simultaneously measuring the mass and mobility of the ion species formed in the ITMS instrument without significant changes to the core ion structures. Using the mass and mobility data acquired with the ITMS/MS/MS instrument in conjunction with density functional theory, the predominant product ions for the various explosives were determined to be $[TNT-H]^-$ for TNT, $[RDX+Cl]^-$ for RDX, $[NO_3]^-$ for EGDN, $[NG+NO_3]^-$ for NG, $[PETN+NO_3]^-$ for PETN, $[HNO_3+NO_3]^-$ for NH_4NO_3, $[HMTD-NC_3H_6O_3+H+Cl]^-$ for HMTD, and $[(CH_3)_2CNH_2]^+$ for TATP. Predominant ionization pathways for the formation of the various product ions include proton abstraction, ion–molecule attachment, autoionization, first-order and multi-order thermolysis, and nucleophilic substitution. The ion trapping scheme in the reaction region of the ITMS instrument has been shown to increase the predominant ion intensities relative to the secondary ion intensities when compared to non-ion trap operation.

The overall objective of the research is to develop a fundamental understanding of the gas phase ionization processes in the ITMS based ETD to facilitate the advancement of its operational effectiveness as well as guide the development of next generation ETDs. A future effort will involve using the ITMS/MS/MS instrument to characterize the ion species formed during the analysis of various fuel–oxidizer mixtures, explosive compositions, and chemical interfering agents. It is projected that this data will lead to advances in the detection algorithms of not only ITMS based ETDs but any ETD that utilizes atmospheric pressure ionization, including MS based systems. The detection algorithm advances are expected to include increased number of explosive types detected as well as decreased false response rates.

Acknowledgments

JK was funded through an interagency agreement between the US Department of Homeland, Security Science and Technology Directorate, Transportation Security Laboratory and the Naval Research Laboratory under IAA no. HSHQDC-10-X-00444. JK acknowledges David Atkinson, Robert Ewing, and Inho Cho for insightful discussion and Pamela Beresford for editing the manuscript. This research was supported in part by appointments for Dr. Tomlinson-Phillips and Dr. Brauer to the Transportation Security Laboratory Visiting Scientist Program administered by the Oak Ridge Institute for Science and Education (ORISE) through an interagency agreement between the US Department of Energy (DOE) and the US Department of Homeland Security. ORISE is managed by Oak Ridge Associated Universities (ORAU) under DOE Contract no. DE-AC05-06OR23100. The US Department of Homeland Security, Science and Technology Directorate, Transportation Security Laboratory sponsored this work under an interagency agreement with ORISE, no. HSHQDC-06-X-00329.

Appendix A. Supporting information

Supplementary data associated with this article can be found in the online version at http://dx.doi.org/10.1016/j.talanta.2012.07.030.

References

[1] D.D. Fetterolf, T.D. Clark, J. Forensic Sci. 38 (1993) 28–39.
[2] R.G. Ewing, D.A. Atkinson, G.A. Eiceman, G.J. Ewing, Talanta 54 (2001) 515–529.
[3] D.S. Moore, Rev. Sci. Instrum. 75 (2004) 2499.
[4] G.A. Eiceman, J.A. Stone, Anal. Chem. 76 (2004) 390A–397A.
[5] G.A. Eiceman, Z. Karpas, Ion Mobility Spectrometry, 2nd ed., CRC Press Taylor & Francis Group, Boca Raton, FL, 2005.
[6] C.J. Proctor, J.F.J. Todd, Anal. Chem. 56 (1984) 1794–1797.
[7] L.L. Danylewych-May, in: Proceedings of the 1st International Symposium on Explosive Detection Technology, Atlantic City, NJ, 1991, pp. 672–686.
[8] V. Bocos-Bintintan, A. Brittain, C.L.P. Thomas, Analyst 126 (2001) 1539–1544.
[9] K.A. Daum, D.A. Atkinson, R.G. Ewing, Talanta 55 (2001) 491–500.
[10] K.A. Daum, D.A. Atkinson, R.G. Ewing, Int. J. Mass Spectrom. 214 (2002) 257–267.
[11] A.J. Marr, D.M. Groves, Int. Soc. Ion Mob. Spectrom. 6 (2003) 59–62.
[12] J. Kozole, J.R. Stairs, I. Cho, J.D. Harper, S.R. Lukow, R.T. Lareau, R. DeBono, F. Kuja, Anal. Chem. 83 (2011) 8596–8603.
[13] A. Jenkins, US Patent 5,200,614, April 6, 1993.
[14] A. Jenkins, W.J. McGann, US Patent 5,491,337, February 13, 1996.
[15] A. Kanu, C. Wu, H. Hilljr, Anal. Chim. Acta 610 (2008) 125–134.
[16] A.W. Szumlas, D.A. Rogers, G.M. Hieftje, Rev. Sci. Instrum. 76 (2005) 086108.
[17] J. Puton, A. Knap, B. Siodłowski, Sens. Actuators B 135 (2008) 116–121.
[18] C.S. Hoaglund, S.J. Valentine, D.E. Clemmer, Anal. Chem. 69 (1997) 4156–4161.
[19] D. Douglas, J. French, J. Am. Soc. Mass Spectrom. 3 (1992) 398–408.
[20] A. Sysoev, A. Adamov, J. Viidanoja, R.A. Ketola, R. Kostiainen, T. Kotiaho, Rapid Commun. Mass Spectrom. 18 (2004) 3131–3139.

[21] A. Krutchinsky, I. Chernushevich, V. Spicer, W. Ens, K. Standing, J. Am. Soc. Mass Spectrom. 9 (1998) 569–579.
[22] K. Tang, A.A. Shvartsburg, H.-N. Lee, D.C. Prior, M.A. Buschbach, F. Li, A.V. Tolmachev, G.A. Anderson, R.D. Smith, Anal. Chem. 77 (2005) 3330–3339.
[23] A. Frisch, H.P. Hratchian, R.D.D. II, T.A. Keith, J. Millam, A.B. Nielsen, A.J. Holder, J. Hiscocks, GaussView 5 Reference, Gaussian, Inc., Wallingford, 2009.
[24] Gaussian 09, Revision A.1, M.J. Frisch, G.E. Scuseria, M.A. Robb, J.R. Cheeseman, G. Scalmani, V. Barone, B. Mennucci, G.A. Petersson, H. Nakatsuji, M. Caricato, X. Li, H.P. Hratchian, A. F. Izmaylov, J. Bloino, G. Zheng, J.L. Sonnenberg, M. Hada, M. Ehara, K. Toyota, R. Fukuda, J. Hasegawa, M. Ishida, T. Nakajima, Y. Honda, O. Kitao, H. Nakai, T. Vreven, J.A. Montgomery, Jr., J.E. Peralta, F. Ogliaro, M. Bearpark, J.J. Heyd, E. Brothers, K.N. Kudin, V.N. Staroverov, R. Kobayashi, J. Normand, K. Raghavachari, A. Rendell, J. C. Burant, S.S. Iyengar, J. Tomasi, M. Cossi, N. Rega, J.M. Millam, M. Klene, J.E. Knox, J.B. Cross, V. Bakken, C. Adamo, J. Jaramillo, R. Gomperts, R.E. Stratmann, O. Yazyev, A.J. Austin, R. Cammi, C. Pomelli, J.W. Ochterski, R.L. Martin, K. Morokuma, V.G. Zakrzewski, G.A. Voth, P. Salvador, J.J. Dannenberg, S. Dapprich, A.D. Daniels, Ö. Farkas, J.B. Foresman, J.V. Ortiz, J. Cioslowski, D.J. Fox., Gaussian, Inc., Wallingford, CT, 2009.
[25] E.D. Glendening, A.E. Reed, J.E. Carpenter, F. Weinhold, NBO Version 3.1.
[26] G. Kaur-Atwal, G. O'Connor, A.A. Aksenov, V. Bocos-Bintintan, C.L. Paul Thomas, C.S. Creaser, Int. J. Ion Mob. Spectrom. 12 (2009) 1–14.
[27] G.E. Spangler, in: Proceedings of the Third International Workshop on Ion Mobility Spectrometry, Galveston, TX, 1995, pp. 115–133.
[28] A. Good, D.A. Durden, P. Kebarle, J. Chem. Phys. 52 (1970) 212–221.
[29] S.L. Chong, J. Ransom, A. Myers, J.L. Franklin, J. Chem. Phys. 56 (1972) 2427–2430.
[30] R.G. Ewing, M.J. Waltman, D.A. Atkinson, Anal. Chem. 83 (2011) 4838–4844.
[31] G.A. Eiceman, D. Preston, G. Tiano, J. Rodriguez, J.E. Parmeter, Talanta 45 (1997) 57–74.
[32] C. OOmmen, S.R. Jian, J. Hazard. Mater. A67 (1999) 253–281.
[33] J.C. Oxley, J.L. Smith, H. Chen, Propellants, Explos., Pyrotech. 27 (2002) 209–216.
[34] J.C. Oxley, J.L. Smith, H. Chen, E. Cioffi, Thermochim. Acta 388 (2002) 215–225.
[35] G.E. Spangler, P.A. Lawless, Anal. Chem. 50 (1978) 884–892.
[36] M. Tam, H.H. Hill, Anal. Chem. 76 (2004) 2741–2747.
[37] G.E. Spangler, J.P. Carrico, S.H. Kim, in: Proceedings of the International Symposium on Analysis and Detection of Explosives, FBI Academy, Quantico, VA, 1983, pp. 267–282.
[38] D. Chakraborty, R.P. Muller, S. Dasgupta, W.A. Goddard III, J. Comput.-Aided Mater. Des. 8 (2001) 203–212.
[39] M.H. Liu, G.F. Zheng, J. Theor. Comput. Chem. 6 (2007) 341–352.
[40] A.C. Landerville, I.I. Oleynik, C.T. White, Shock Compression Condens. Matter (2009) 813–816.
[41] W.L. Ng, J.E. Field, H.M. Hauser, J. Appl. Phys. 59 (1986) 3945–3952.
[42] M.A. Hiskey, K.R. Brower, J.C. Oxley, J. Phys. Chem. 95 (1991) 3955–3960.
[43] M. Li, G. Wang, X. Guo, Z. Wu, H. Song, J. Mol. Struct.: Theochem 900 (2009) 90–95.
[45] G.R. Asbury, J. Klasmeier, H.H Hill Jr., Talanta 50 (2000) 1291–1298.
[46] E. Arunan, G.R. Desiraju, R.A. Klein, J. Sadlej, S. Scheiner, I. Alkorta, D.C. Clary, R.H. Crabtree, J.J. Dannenberg, P. Hobza, H.G. Kjaergaard, A.C. Legon, B. Mennucci, D.J. Nesbitt, Pure Appl. Chem. 83 (2011) 1619–1636.
[47] R. Gunawan, D. Zhang, J. Hazard. Mater. 165 (2009) 751–758.
[48] S. Chang, H. Ko, S. Singamaneni, R. Gunawidjaja, V.V. Tsukruk, Anal. Chem. 81 (2009) 5740–5748.
[49] J. Tomlinson-Phillips, J. Kozole, C.S. Brauer, A. Wooten, J. Harper, J. Stairs, in: Proceedings of the Gordon Research Conference Detecting Illicit Substances: Explosives & Drugs, Lucca, Italy, 2011.
[50] C.K. Hilton, C.A. Krueger, A.J. Midey, M. Osgood, J. Wu, C. Wu, Int. J. Mass Spectrom. 298 (2010) 64–71.
[51] A.H. Lawrence, P. Neudorfl, Anal. Chem. 60 (1988) 104–109.
[52] T.L. Buxton, P.d.B. Harrington, Anal. Chim. Acta 434 (2001) 269–282.